ASTRONOMY
AND
ASTROPHYSICS

The Galactic metallicity gradient

W.R.J. Rolleston[1]**, S.J. Smartt**[2,3]**, P.L. Dufton**[1,⋆]**, and R.S.I. Ryans**[1]

[1] Department of Pure and Applied Physics, The Queen's University of Belfast, Belfast BT7 1NN, N. Ireland, UK (R.Rolleston@qub.ac.uk)
[2] The Isaac Newton Group of Telescopes, Apartado de Correos 368, 38780 Santa Cruz de La Palma, Canary Islands, Spain
[3] Institute of Astronomy, University of Cambridge, Madingley Road, Cambridge, CB3 0HA, England, UK

Abstract. We have previously published intermediate to high resolution spectroscopic observations of approximately 80 early B-type main-sequence stars situated in 19 Galactic open clusters/associations with Galactocentric distances distributed over $6 \leq R_g \leq 18$ kpc. This current study collates and re-analyses these equivalent-width datasets using LTE and non-LTE model atmosphere techniques, in order to determine the stellar atmospheric parameters and abundance estimates for C, N, O, Mg, Al and Si. The latter should be representative of the present-day Galactic interstellar medium. Our extensive observational dataset permits the identification of sub-samples of stars with similar atmospheric parameters and of homogeneous subsets of lines. As such, this investigation represents the most extensive and systematic study of its kind to date.

We conclude that the distribution of light elements (C, O, Mg & Si) in the Galactic disk can be represented by a linear, radial gradient of -0.07 ± 0.01 dex kpc^{-1}. Our results for nitrogen and oxygen viz. (-0.09 ± 0.01 dex kpc^{-1} and -0.067 ± 0.008 dex kpc^{-1}) are in excellent agreement with that found from the study of H II regions. We have also examined our datasets for evidence of an abrupt discontinuity in the metallicity of the Galactic disk near a Galactocentric distance of 10 kpc (see Twarog et al. 1997). However, there is no evidence to suggest that our data would be better fitted with a two-zone model. Moreover, we observe a N/O gradient of -0.04 ± 0.02 dex kpc^{-1} which is consistent with that found for other spiral galaxies (Vila-Costas & Edmunds 1993).

Key words: stars: abundances – stars: early-type – Galaxy: abundances – Galaxy: evolution

1. Introduction

The chemical evolution of the interstellar medium (ISM) varies between galaxies and is both position and time dependent within a galaxy. For example, metallicity studies of objects in the Magellanic Clouds (see Rolleston et al. 1993b, 1996) demonstrate that the global environments of these dwarf, irregular galaxies are completely different to that of the Milky Way. Furthermore,

studies of young, B-type stars in Galactic clusters/associations and field FG-type dwarfs have shown the metal content of the ISM to differ by up to 0.5 dex over relatively small (1 kpc) spatial scales (see Rolleston et al. 1994; Edvardsson et al. 1993). Temporal variations have also been investigated and an age-metallicity relationship has been constructed using observations of the Galactic globular cluster and open cluster systems (see, for example, Strobel 1991; Carraro & Chiosi 1994). These variations are a consequence of successive generations of stars having enriched the ISM with products of nucleosynthesis that were generated in their cores. Thus, abundance investigations provide a key to understanding the formation and chemical evolution of galaxies.

However, theoretical models of the chemical and dynamical evolution of the Galaxy depend on many variables including the historical star formation rate (Phillipps & Edmunds 1991), the initial mass function (Güsten & Metzger 1982), radial inflows/outflows of gas (Mayor & Vigroux 1981) and the infall of metal-poor gas from the Galactic halo (Pilyugin & Edmunds 1996; van den Hoek & de Jong 1997). The radial variations of metallicity within the Galactic disk (ie. abundance gradients) predicted by such models are not tightly constrained. Thus, the reliable determination of the extent and magnitude of radial and spatial variations for a wide range of elements must be used to constrain models of disk evolution (see, for example, Matteucci & Francois 1989; Edmunds & Greenhow 1995; Prantzos & Aubert 1995, Portinari & Chiosi 1999).

Considerable effort has been invested in studying metallicity variations within our Galaxy and external galaxies. The existence of large-scale abundance gradients were first established by Searle (1971) in a survey of H II regions in six late-type spiral (Sc) galaxies (see also Garnett et al. 1997, for a recent review and comparison of abundance gradients in normal spiral galaxies). Early investigations of a metallicity gradient in the Galactic disk included the photometric studies of old open clusters (Janes 1979) and evolved disk stars (Mayor 1976). However, most information concerning radial abundance gradients have been derived from the spectroscopic investigation of H II regions (Pagel & Edmunds 1981; Shaver et al. 1983; Afflerbach et al. 1997) and planetary nebulae (Torres-Peimbert & Peimbert 1977; Maciel & Köppen 1994), as observations of these bright, gaseous nebulae are relatively easy to obtain. Such large-scale

---

Table 1. A compilation of observed radial metallicity gradients in the Galactic disk, grouped by object type, is presented. Where more than one element is sampled, the value of the gradient is either the mean or a representative value of all the elements in that study. This list is not meant to be an exhaustive catalogue of individual gradients derived by each author for each element, but an illustration of work already undertaken. The more important comparisons are discussed in Sect. 6, and the reader is referred to the references below for details of each result.

Object	Age (Myr)	R_g (kpc)	Element	Gradient (dex kpc^{-1})	Reference
Open clusters:	$\leq 10^4$	6–16	Fe	-0.05	Janes (1979)
		7–11	Fe	-0.09	Panagi & Tosi (1981)
		7–10	Fe	-0.11	Cameron (1985)
		8–15	Fe	-0.09	Friel & Janes (1993)
		6–16	Fe	-0.07	Twarog et al. (1997)
dF/dG Field stars:	$\leq 10^4$	8–12	Fe	-0.05	Mayor (1976)
Cepheids:	10^3–10^4	5–15	Fe	-0.07	Harris (1981)
GK-supergiants:	$\leq 10^2$	8–11	Fe	-0.13	Luck (1982)
AF-type stars:	10–10^2	10–13	Fe	-0.08	Christian & Smith (1983)
Planetary nebulae:	10^3–10^4	8–13	O	-0.06	Torres-Peimbert & Peimbert (1977)
		2–14	N, O, Ne	-0.04	Pasquali & Perinotto (1993)
		4–13	N, Ne, S, Ar	-0.06	Maciel & Köppen (1994)
		4–13	O, Ne, S, Ar	-0.06	Maciel & Quireza (1999)
H II regions:	≤ 10	8–14	N, O	-0.16	Peimbert et al. (1978)
		4–14	N, O, Ne, S, Ar	-0.07	Shaver et al. (1983)
		1–10	N, Ne, S	-0.08	Simpson et al. (1995)
		4–11	O	-0.05	Afflerbach et al. (1996)
		12–18	N, O, S	-0.02	Vílchez & Esteban (1996)
		0–12	N, O, S	-0.07	Afflerbach et al. (1997)
		13–17	N, S	-0.10	Rudolph et al. (1997)
B-type stars:	$\leq 10^2$	6–13	O	-0.03	Fitzsimmons et al. (1992)
		7–13	N, O	> -0.02	Kaufer et al. (1994)
		7–15	C, N, O, Mg, Al, Si	> -0.03	Kilian-Montenbruck et al. (1994)
		5–14	C, N, O, Mg, Al, Si	> -0.07	Gummersbach et al. (1998)

gradients now appear to be well established in both our Galaxy and in other spiral galaxies (see, for example, the recent reviews by Pagel 1997 and McWilliam 1997). In Table 1, an overview is given of published estimates for the magnitudes of the abundance gradients. It should be noted that this compilation is not meant to be exhaustive, but rather a selection that is representative of that which can be found in the literature.

However, relatively few elements have been studied in a homogeneous and consistent manner to date and the precise behaviour as a function of Galactocentric radius (R_g) is still rather uncertain. For example, Shaver et al. (1983) found radial abundance variations of approximately -0.07 dex kpc^{-1} for oxygen, nitrogen and argon from a study of 67 H II regions within the range of Galactocentric distances, 4.0–12.5 kpc – with some evidence for a steepening of the gradient towards the inner region ($R_g < 6$ kpc). This contrasts with the results of the photometric study of intermediate age clusters by Janes (1979), which indicated that the gradient steepened in the outer Galactic disk (at $R_g > 9$ kpc). More recently, Twarog et al. (1997) have suggested that the metallicity distribution of clusters as a function of Galactocentric distance is best described by distinct zones (and a discontinuity), rather than a continuous linear decline in metallicity. Given that the metallicity studies

of H II regions and intermediate-to-old clusters sample different epochs in the Galaxy's history, it is essential that one relates results from comparable objects when attempting to correlate the data.

2. B-type stars as tracers of Galactic chemical composition

Early-type stars provide an excellent method for probing the metallicity and recent evolutionary history of both the Milky Way and external galaxies. As a direct consequence of their high luminosities, early B-type dwarfs can be observed in distant regions of the Galaxy at high spectral resolution and at a high signal-to-noise ratio. Such stars have evolutionary ages typically less than 30 Myr and possess photospheres that are *not normally* contaminated by core-processed material (see Gies & Lambert 1992). Furthermore, B-type dwarfs exhibit relatively rich, photospheric metal-line spectra with absorption features due to C, N, O, Mg, Si, S, Al and Fe. In addition, the spectral lines are mostly well separated; thus aiding the identification of line-free regions, essential for the determination of reliable equivalent widths for the abundance calculations. Hence, these objects should provide unambiguous information on the *present-day* chemical composition of the ISM within the parent galaxy.

Such studies should also not be subject to systematic errors that may be introduced by other methods. The analyses of diffuse, emission-line nebulae may suffer from chemical fractionation processes such as grain formation (see Henning & Gürtler 1986) and element diffusion (see Bahcall & Pinsonneault 1995) such that the measured abundances will not reflect the true composition of the gas cloud. In particular the former problem creates large uncertainties in the abundances derived for refractory elements (eg. C, Si and Fe) which are particularly susceptible to grain depletion.

There have been several attempts to measure the magnitude of radial abundance gradients using young, B-type dwarfs as tracers of metallicity in the Galactic disk. The first attempt was by Gehren et al. (1985), who found an essentially flat relation (zero gradient) for oxygen and nitrogen. Similarly, Fitzsimmons et al. (1990, 1992) did not detect any systematic abundance variations. Although these studies extensively sampled the region within $\sim$2 kpc from the Sun, viz. the Sagittarius, Local and Perseus spiral arms, they failed to adequately survey the outer disk beyond the Perseus spiral arm ($R_{\mathrm{g}} \sim 11$ kpc). Furthermore, a shallow gradient may indeed be representative of the solar neighbourhood (see Sect. 6.4), and element depletion may not occur until one reaches the Perseus arm and beyond. More recently, other groups including Kaufer et al. (1994) and Kilian-Montenbruck et al. (1994) made revised attempts of estimating the Galactic abundance gradient. However, several factors have almost certainly contributed to the small gradients inferred from these stellar studies, viz. the statistical limitations imposed by using very small samples, and errors in distance estimates or element abundances in the critical data-points at large Galactocentric distances. The study by Smartt & Rolleston (1997) was the first to establish a significant Galactic abundance gradient of oxygen using early-type stars. This investigation involved the analysis of some 50 stars from 18 young stellar clusters and associations with Galactocentric distances ranging from $6 \leq R_{\mathrm{g}} \leq 18$ kpc; furthermore, it adequately sampled the outer Galactic disk. Smartt & Rolleston (1997) derived an oxygen abundance gradient of -0.07 ± 0.01 dex kpc^{-1}, showing the first agreement of such stellar studies with Galactic H II region and PN results. Further, explanations were given in this latter paper as to why previous attempts at measuring stellar abundance gradients found null results. More recently, Gummersbach et al. (1998) have re-analysed a slightly extended observational dataset of Kaufer et al. (1994) and found that errors inherent in their previous analysis did indeed contribute to the derivation of a flat gradient.

In this paper, we use our extensive observational dataset of early B-type stars in Galactic disk, open clusters and associations to derive estimates of abundance gradients for additional elements, viz. C, N, Mg, Al & Si. Unfortunately, it was not possible to derive S & Fe abundances for a statistically significant sample of stars, due to the weakness of the S II, S III and the Fe III features. Sources of the observational data (stellar atmospheric parameters, distances, metal-line equivalent widths) are described in Sect. 3. The analysis of the equivalent width datasets were undertaken using LTE and non-LTE techniques, and these methods are described in Sect. 4 and Sect. 5 respectively, with the results being discussed in Sect. 6.

3. Source of spectroscopic data

The observational datasets utilized in this paper comprise high-resolution spectroscopy ($R \sim 10\,000$–$40\,000$) of 80 stars in 19 Galactic disk, open clusters/associations. This represents the progress of approximately 15 years of an observational campaign and includes objects with Galactocentric distances distributed throughout the range $6.0 \leq R_{\mathrm{g}} \leq 17.6$ kpc. In Table 2, we summarize the source of the individual spectroscopic datasets – providing references for the stellar atmospheric parameters and metal-line equivalent widths, and the primary sources of the cluster and stellar distance estimates. Smartt et al. (1996b, 1996c) demonstrated that using a homogeneous set of stars (with similar atmospheric parameters) permits a detailed and reliable analysis of spatial and radial abundance variations to be undertaken. Indeed, with a few refinements (as discussed in Sect. 4), such a homogeneous set of stars can be extracted from our observational datasets. The 22 objects listed in Table 2 include 3 Galactic disk field stars; however, for simplicity throughout this paper we will refer to the 22 objects generically as clusters.

4. LTE abundance analysis

The methods used in the derivation of the LTE stellar atmospheric parameters are similar to those previously discussed in Dufton et al. (1990a) and Hambly et al. (1997). Primarily, the theoretical computations were based on the grid of line-blanketed model atmospheres of Kurucz (1991), together with LTE radiative-transfer codes to derive the atmospheric parameters and chemical compositions. The atomic data were as discussed in Jeffery (1996). Further details on the individual derivations of the stellar parameters can be found in the papers referenced in Table 2. It should be noted that a subsequent non-LTE analysis of selected elements was undertaken (see Sect. 5), in order to estimate the magnitude of uncertainties inherent in the LTE abundance gradients due to the neglect of non-LTE effects.

Given the merits of using a homogeneous set of stars (with similar effective temperatures and surface gravities, together with comparable equivalent width datasets), we have invested considerable effort in addressing possible sources of inhomogeneities in our sample. For example, the full dataset comprises stars with effective temperatures spanning the range 17 500–33 500 K, while the size of the individual equivalent width datasets increases with the epoch of the observations (as a result of technological advances). Furthermore, the original estimates of the stellar effective temperatures made use of both photometric and spectroscopic techniques, whilst it was not always possible to determine a value for the microturbulence, ξ. Hence, we have considered the effects of such possible inhomogeneities within our sample on the derived elemental abundance gradients, and (where appropriate) we have identified sub-samples

Table 2. Source of spectroscopic data (references).

Cluster	Stellar parameters/metal-line equivalent widths	Distance estimates (if different)
NGC 6611	Brown et al. (1986b)	Thé et al. (1990)
NGC 6231	Lennon & Dufton (1983)	Shobbrook (1983b)
NGC 6531	Brown et al. (1986a)	Knude (1992)
NGC 4755	Brown et al. (1986a)	Shobbrook (1984)
IC 2944	Brown et al. (1986a)	Becker & Fenkart (1971)
Loose Assoc.	Brown et al. (1986a)	Dufton (1979)
NGC 3293	Brown et al. (1986a)	Shobbrook (1983a)
Cepheus OB III	Dufton et al. (1990a)	Crawford & Barnes (1970)
NGC 2362	Brown et al. (1986a)	Becker & Fenkart (1971)
Berkeley 94	Dufton et al. (1994)	Fitzsimmons (1993)
h +χ Per	Dufton et al. (1990a)	Shobbrook (1980)
NGC 457	Dufton et al. (1994)	Fitzsimmons (1993)
RLWT 41	Smartt et al. (1996b, 1996c)	–
Wat 1	Smartt et al. (1996b, 1996c)	–
S 285	Rolleston et al. (1994)	–
RLWT 13	Smartt et al. (1996b, 1996c)	–
Bochum 1	Rolleston et al. (1993a)	Fitzsimmons (1993)
Dolidze 25	Lennon et al. (1991)	Moffat & Vogt (1975)
NGC 1893	Rolleston et al. (1993a)	Fitzsimmons (1993)
MR 1	Smartt et al. (1996a)	–
S 289	Smartt et al. (1996b, 1996c)	–
S 283	Smartt et al. (1996b, 1996c)	–

of homogeneous stars. Below we discuss these considerations in turn.

4.1. The full sample

As a first approach, we have considered the entire stellar sample. The adopted atmospheric parameters were used to deduce LTE abundance estimates for all the observed metal-line features for which atomic data were included in our line-formation codes. This comprised 4 C II lines, 10 N II lines, 31 O II lines, 1 Mg II line, 3 Al III lines and 6 Si III lines. Mean elemental abundances per star were deduced by taking the arithmetic mean of the estimates obtained from individual lines of the same species. Similarly, a mean cluster abundance was derived from the mean element abundances of individual stars. In the model atmosphere calculations, we assumed a value for the microturbulence of 5 km s^{-1} which has been found previously to be appropriate from similar LTE analyses of B-type dwarfs (see Hardorp & Scholz 1970; Gies & Lambert 1992).

4.2. Homogeneous subsets of lines

The spectroscopic observations were obtained over a 15 year period. During this time, there have been significant technological advances with IPCS detectors being superseded by high relative quantum efficiency and large format CCD's. Furthermore, it is now routine to obtain high-resolution spectra ($R \sim 40\,000$) and complete wavelength coverage of faint stars with échelle spectrographs on 4-m class telescopes. The above have led to different completeness levels of the metal-line equivalent width datasets for stars observed at different epochs. Hence,

we have attempted to define a homogeneous subset of lines using the following criteria. First, we only considered those unblended transitions of N, O, Al & Si that were observed in over 66% of the stellar sample. Secondly, we included additional lines from the same multiplets as those of the primary O II lines. For C, no lines satisfied the first criterion and so the blue and red lines were considered independently, while only one Mg II feature was observed in the $\lambda\lambda 3900$–4750 Å region. Thus, our subset of lines for each element include 3 Carbon (C II 3920.69, 6578.10, 6582.90), 7 Nitrogen (N II 3995.00, 4601.48, 4607.16, 4613.87, 4621.29, 4630.54, 4643.09), 15 Oxygen (O II 3912.00, 3945.04, 3954.87, 3982.72, 4072.16, 4078.84, 4092.93, 4132.80, 4590.97, 4596.18, 4638.86, 4649.14, 4650.84, 4661.63, 4676.24), 1 Magnesium (Mg II 4481.23), 1 Aluminium (Al III 4528.91) and 3 Silicon (Si III 4552.62, 4567.82, 4574.76) features.

4.3. Homogeneous subsets of stars selected by temperature constraints

Fitzsimmons et al. (1990) demonstrated that errors in the abundance estimates, due to uncertainties in the atmospheric parameters, could be reduced by restricting the sample of stars to those with effective temperatures similar to that corresponding to the maximum line-strength of a particular ion. Our sample of 80 stars display effective temperatures within the range 17 500–33 500 K with a mean temperature of $\overline{T_{\text{eff}}} = 25\,275 \pm 3\,750$ K. Furthermore, the objects are all (near) main-sequence stars and the mean logarithmic surface gravity of stars in our sample is $\overline{\log g} = 4.02 \pm 0.25$ dex. Therefore, for each species under consideration and for a surface gravity of $\log g = 4.0$, we deter-

mined the temperature ($T_{\max}$) corresponding to the maximum line-strength, viz. 23 500 K (C II), 25 000 K (N II), 27 500 (O II), 24 000 (Al III) and 25 000 K (Si III). For all the species studied, the selection of stars with effective temperatures in the range $|T_{\mathrm{eff}} - T_{\max}| \leq 5\,000$ K and $|T_{\mathrm{eff}} - T_{\max}| \leq 3\,000$ K led to errors in the abundance estimates of less than 0.16 dex and 0.13 dex respectively for errors in the effective temperature of $\pm 1\,000$ K. We therefore investigated the effect on the estimates of abundance gradients for the afore-mentioned species using such sub-samples of stars. For the Mg II 4481 Å feature, the line-strength peaks at a temperature around 10 000 K which is considerably cooler than any of the stars in our sample. Hence, for this ion we arbitrarily considered subsets of stars within $\pm 5\,000$ K and $\pm 3\,000$ K of the mean effective temperature of the stellar sample, viz. $\overline{T_{\mathrm{eff}}} \sim 25\,000$ K.

4.4. Photometric and spectroscopic temperatures

Ideally, the atmospheric parameters should be derived for all stars using similar techniques. However, for the determination of the stellar effective temperature, in particular, this was not always possible. For example, spectroscopic temperatures for early B-type stars can be deduced from the relative strengths of lines from two ionization stages of silicon such as Si III/Si IV (see Smartt et al. 1996b). Unfortunately, it was not always possible to reliably measure equivalent widths of lines from two ionization stages of silicon due to a number of factors. First, if the stellar temperature is sufficiently far from the temperature corresponding to the maximum line-strength of the ion, and/or the photospheric composition was of lower metallicity, the absorption features are intrinsically weak. Secondly, for those stars that exhibit large projected rotational velocities, the lines are often blended with other features or one requires much higher S/N to discriminate them from the stellar continuum. Furthermore, the Si II lines are subject to relatively strong non-LTE effects; hence, it was only possible to use (where available) the Si III/Si IV ionization equilibrium to yield spectroscopic temperatures in the LTE analysis.

Photometric temperature estimates were obtained from the Strömgren reddening free $[u - b]$ index using the calibration of Napiwotzki et al. (1993), which is appropriate for main-sequence stars. However, it is important to establish whether the different methods for deriving effective temperature estimates could introduce a bias in the derived abundance gradients. Hence, we evaluated abundance gradients for two sub-samples of stars corresponding to those with temperatures derived using spectroscopic and photometric techniques. For bright, normal B-type stars in the solar neighbourhood, Hambly et al. (1997) did not find evidence for systematic differences between temperatures derived using Strömgren indices and the Si III/Si IV ionization equilibrium.

4.5. Microturbulence, ξ

As discussed in Sect. 4.1, we initially adopted a value of 5 km s^{-1} for the microturbulence parameter in all the pro-

gramme stars. For approximately 25% of the sample, it was possible to estimate a value for the microturbulent velocity by adjusting this parameter so as to remove the dependence of the derived O II abundance upon line-strength (see, for example, Gies & Lambert 1992). This method yielded a mean microturbulence of 7.2±3.2 km s^{-1} for the sub-sample of stars. No temperature dependence on the derived value of ξ was observed; however, for 3 stars in $h + \chi$ Per which are evolving off the main-sequence ($\log g \sim 3.7$ dex), we measured larger values (~ 12 km s^{-1}) for the microturbulent velocity. Excluding the latter 3 objects, we found a mean value of $\xi = 6.2 \pm 2.0$ km s^{-1}. We therefore investigated the possible effects of the afore-mentioned assumption on the resultant abundance gradients, by adopting our derived values of microturbulence for the 25% of the sample and a value of 5 km s^{-1} for the remaining objects.

4.6. Galactocentric distance

Distance estimates to the Galactic clusters and associations can be derived using either photometric or spectroscopic techniques. The photometric method employs the fitting of theoretical isochrones to the observed colour-magnitude diagrams and colour-colour diagrams (see, for example, Fitzsimmons 1993); hence, this approach will provide reliable results for those clusters which possess well populated main-sequences. For the objects within the Sagittarius, Local and Perseus spiral arms and the two more distant clusters Bochum 1 and NGC 1893, this criterion was certainly applicable. Therefore for these objects, we primarily adopted values of Galactocentric distance (R_{g} – see Table 3) that were based on photometric distance estimates.

However, our most distant targets are generally associated with H II regions which are sparsely populated (see, for example, Turbide & Moffat 1993) and the main-sequence fitting technique yields distance estimates with rather large uncertainties. Similarly, large uncertainties exist in the photometric distance estimates of isolated field stars. Thus, the derived atmospheric parameters for the 3 field stars and individual stars in the outer Galactic disk H II regions were compared with the evolutionary isochrones of Bertelli et al. (1994); isochrones were selected that were consistent with the observed metallicity of each star. These comparisons yielded stellar masses and luminosities, which were combined with the visual bolometric corrections (Kurucz 1979), the published apparent visual magnitudes and reddenings (see Table 2 for references) to provide individual spectroscopic distance determinations. Mean distance estimates of each cluster/association were calculated using the arithmetic mean of the individual stellar distances. These methods are discussed in detail by, for example, Rolleston et al. (1997).

The adoption of photometric and spectroscopic distances for groups of objects, that are mainly distributed in the solar neighbourhood and outer disk respectively, could potentially introduce a bias into the derived abundance gradients. Hence, we also analyzed our dataset using spectroscopic distances for all targets.

Table 3. LTE metal abundances are presented for our 19 Galactic disk, open clusters/associations and 3 disk, field stars (viz. RLWT 41, RLWT 13 and MR 1). The number in brackets after each abundance (n) refers to the number of stars upon which the mean abundance estimates were based. Where $n > 1$, the quoted error is the standard deviation of the mean stellar abundances and where $n = 1$, this refers to the standard deviation of the mean element abundance as determined from the individual lines.

Cluster	$R_{\rm g}$ (kpc)	Carbon		Nitrogen		Oxygen		Magnesium		Aluminium		Silicon	
						$12 + \log[X/H]\ (n)$							
NGC 6611	6.06±0.27	8.22±0.30	(1)	7.87±0.28	(2)	8.88±0.14	(4)	7.44±0.30	(1)	6.22±0.30	(1)	7.64±0.35	(4)
NGC 6231	6.88±0.19	—		7.96±0.26	(6)	—		8.03±0.32	(4)	—		—	
NGC 6531	7.28±0.29	—		8.27±0.07	(2)	8.84±0.18	(1)	7.85±0.30	(1)	6.37±0.30	(1)	7.78±0.09	(1)
NGC 4755	7.63±0.04	7.98±0.09	(2)	7.76±0.37	(6)	8.86±0.12	(6)	8.01±0.21	(2)	—		7.36±0.17	(2)
IC 2944	7.88±0.04	—		7.95±0.00	(2)	8.85±0.07	(3)	8.00±0.14	(2)	6.51±0.04	(2)	7.48±0.22	(3)
Loose Assoc.	8.13±0.05	—		8.10±0.30	(1)	8.88±0.07	(2)	8.00±0.30	(1)	6.35±0.30	(1)	7.76±0.09	(2)
NGC 3292	8.19±0.02	7.78±0.30	(1)	7.74±0.24	(8)	8.87±0.12	(7)	7.63±0.40	(4)	6.30±0.06	(2)	7.46±0.23	(5)
Cepheus OB III	8.78±0.08	7.63±0.16	(4)	7.56±0.36	(5)	8.79±0.25	(6)	7.40±0.14	(5)	6.06±0.20	(4)	7.46±0.22	(6)
NGC 2362	9.38±0.20	—		8.09±0.14	(3)	8.87±0.02	(3)	7.89±0.12	(3)	6.38±0.30	(1)	7.41±0.04	(3)
Berkeley 94	9.90±0.10	—		7.61±0.30	(1)	8.80±0.16	(3)	7.15±0.25	(5)	6.13±0.07	(2)	7.37±0.26	(5)
$h + \chi$ Per	9.93±0.09	7.96±0.12	(4)	8.01±0.18	(5)	9.26±0.06	(3)	7.61±0.26	(4)	6.47±0.27	(4)	7.52±0.67	(3)
NGC 457	10.4±0.3	8.01±0.40	(4)	7.83±0.30	(1)	—		7.12±0.30	(1)	6.18±0.06	(2)	7.38±0.42	(5)
RLWT 41	10.4±1.0	7.84±0.17	(1)	7.29±0.30	(1)	8.16±0.20	(1)	—		5.95±0.30	(1)	6.80±0.01	(1)
Wat 1	11.6±0.8	7.62±0.09		7.33±0.30	(1)	8.59±0.19	(1)	7.27±0.30	(1)	5.82±0.30	(1)	7.24±0.07	(1)
S 285	12.3±0.3	7.58±0.04		7.78±0.45	(2)	8.86±0.22	(2)	7.46±0.04	(2)	6.08±0.27	(2)	7.68±0.33	(2)
RLWT 13	13.1±1.0	7.40±0.21	(1)	7.24±0.30	(1)	8.50±0.26	(1)	7.32±0.30	(1)	5.86±0.30	(1)	7.09±0.14	(1)
Bochum 1	13.2±0.2	7.74±0.12	(1)	7.62±0.05	(2)	8.58±0.20	(1)	7.34±0.09	(1)	5.99±0.30	(1)	7.45±0.02	(2)
Dolidze 25	13.2±1.2	—		—		8.38±0.24	(1)	—		—		6.80±0.16	(1)
NGC 1893	13.3±0.2	7.54±0.20	(3)	7.36±0.30	(2)	8.81±0.29	(4)	7.23±0.08	(5)	6.06±0.11	(3)	7.29±0.20	(6)
MR 1	15.0±1.5	—		—		8.08±0.03	(1)	—		—		7.14±0.04	(1)
S 289	15.4±0.7	7.44±0.23	(2)	7.16±0.18	(2)	8.37±0.10	(2)	7.12±0.04	(2)	6.10±0.30	(1)	6.79±0.05	(2)
S 283	17.6±1.0	—		7.65±0.30	(1)	8.22±0.17	(1)	7.24±0.30	(1)	6.42±0.30	(1)	7.15±0.04	(1)

4.7. LTE results

Individual stellar and mean cluster abundances were deduced as discussed above for the 'Full sample' and for each of the 'Sub-samples'. These were combined with the estimates of Galactocentric distance to calculate the magnitude of the abundance gradients – by a linear least squares fit through the data points. The fitting routine did not weight the points according to individual errors associated with each star or open cluster/ association, but rather we assumed a standard error of ±0.2 dex. It should be noted that the standard deviations of the mean cluster abundances were generally less than 0.2 dex for those clusters for which individual stellar estimates were obtained for two or more stars. However, such an error estimate may be more realistic of the total uncertainties in our techniques (including, for example, systematic errors which may arise from the assumption of LTE). It should be noted that the effect of including individual errors on the data-points as tabulated in Table 3 did not significantly affect the magnitude or the associated errors of the derived gradients.

The use of different sets of stars and/or stellar features as described in Sect. 4.1 to Sect. 4.6, led to the following general conclusions. First, the identification of homogeneous subsets of lines did not lead to significantly different gradients (as compared with the full sample), but rather it improved the reliability of the fits. Secondly, the imposition of a temperature constraint to within ±5 000 K of that corresponding to the maximum line-strength of a particular species also served to reduce the uncertainty in the magnitude of the derived gradients without yielding significantly different results. Thirdly, the adoption of both photometric and spectroscopic temperature estimates, the assump-

tion of a value of 5 km s^{-1} for the microturbulence, and the derivation of Galactocentric distances using both photometric and spectroscopic techniques, did not appear to bias the results.

In Table 3, we present the LTE stellar abundances and the adopted Galactocentric distances that have been used to derive the values of the abundance gradients summarized in Table 4 and shown graphically in Fig. 1. The cluster abundances given in Table 3 have been derived using the homogeneous subset of stars with $|T_{\rm eff} - T_{\rm max}| \leq 5\,000$ K (see Sect. 4.3), and for the homogeneous subset of lines listed in Sect. 4.2. Below we discuss the results for each element in turn.

4.7.1. Carbon

The full carbon equivalent width dataset yielded a gradient of -0.08 ± 0.02 dex kpc^{-1}. However, this comprised three distinct subsets of lines, viz. 1) the 3920 Å feature which was observed for 10 clusters with $R_{\rm g}$ between 5–13 kpc, 2) data for the 4267 Å feature which was obtained for 5 clusters ($R_{\rm g} \sim 9$–13 kpc), and 3) the red C II lines which were only observed for objects in the outer Galactic disk ($R_{\rm g} \sim 10$–17 kpc). The C II 4267 Å doublet is known to be susceptible to strong non-LTE effects (see Eber & Butler 1988); furthermore, this equivalent width dataset is only available for a restricted range of Galactocentric distances. Thus, the C II 4267 Å feature was excluded from our analysis. On the other hand, the 3920 Å line and the red C II lines (6578.10, 6582.90 Å) should be reliable. Indeed, the 3920 Å feature alone yields a gradient of -0.07 ± 0.02 dex kpc^{-1}. An analysis of the red lines, which sample the outermost disk regions, include data for a star in the H II region, S 283. However,
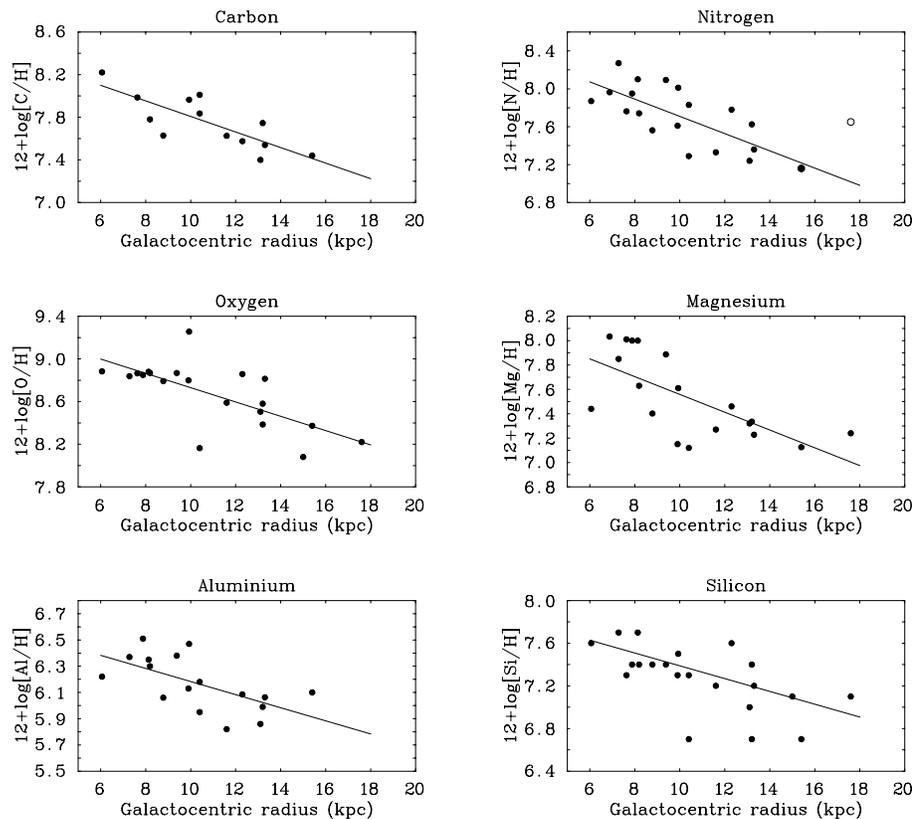
Fig. 1. The variation of element abundances in the present-day Galactic disk as a function of Galactocentric distance. The LTE abundances have been determined for our homogeneous sample of B-type stars (*filled circles*), which are tabulated in Table 3. The *open circle* represents the nitrogen abundance estimate for S 283-2 which was not included in the final analysis (see Sect. 4.7.2). The solid lines represent a linear least-squares fit through the data-points, the results of which are listed in Table 4.

this object maybe peculiar in that it exhibits enhanced C&N abundances relative to its mean photospheric metallicity (see Smartt et al. 1996c, Hibbens et al. 1998). Furthermore, S 283-2 is associated with a region of strong H II emission and the nebular subtraction around the C II red lines was problematic. The inclusion of this object leads to a shallower gradient for carbon (and nitrogen); however, we caution against placing significance on this data-point given the problems above and would encourage higher resolution observations to check the validity of it's carbon abundance in particular. Exclusion of the data-point for S 283 provides a gradient of -0.07 ± 0.03 dex kpc^{-1} as determined from the red lines. Restricting the carbon dataset to those stars within 5 000 K of $T_{\max}$ leads to excellent agreement between the abundance gradient deduced from the 3920 Å and red C II lines – as the effective temperature of S 283-2 does not satisfy this constraint.

We detected no significant differences in the gradients derived using separate sets of stars for which abundance analyses were undertaken using either photometric or spectroscopic indicators. Indeed for carbon, our two subsets of stars with Strömgren and silicon temperatures respectively possess comparable Galactocentric distributions. From our analysis, we also conclude that the assumption of $\xi = 5$ km s^{-1} will introduce an error of less than 0.004 dex kpc^{-1} – which is within our quoted errors. Thus, we conclude that a carbon abundance gradient of -0.07 ± 0.02 dex kpc^{-1} (as derived from the 3920 Å and red C II features) is appropriate for the present-day Galactic disk.

Table 4. LTE abundance gradients: calculated using the homogeneous subset of stars with $|T_{\mathrm{eff}} - T_{\max}| \leq 5\,000$ K (see Sect. 4.3) and the homogeneous subset of lines discussed in Sect. 4.2. $T_{\max}$ corresponds to the temperature at which the metal-line spectrum reaches a maximum line-strength, and N_{lines} is the number of lines used in the determination of the element abundance gradients.

Element	Gradient (dex kpc^{-1})	$T_{\max}$ (K)	N_{lines}
C	-0.07 ± 0.02	23 500	3
N	-0.09 ± 0.01	25 000	7
O	-0.067 ± 0.008	27 500	15
Mg	-0.07 ± 0.01	25 000	1
Al	-0.050 ± 0.015	24 000	1
Si	-0.06 ± 0.01	25 000	3

4.7.2. Nitrogen

The analysis of the complete nitrogen equivalent width dataset yields a gradient of -0.05 dex kpc^{-1}. However, this value may be biased by the inclusion of red N II lines for the outermost clusters. Only one line (viz. N II 3995 Å) fulfills our selection criterion for the identification of a homogeneous set of lines. This absorption feature is observed in over 90% of our sample; hence, an estimate of the nitrogen gradient using this feature should be reliable. Indeed, using the temperature restricted subsample of stars with $|T_{\mathrm{eff}} - T_{\max}| \leq 5\,000$ K, we derive a nitrogen abundance gradient of -0.07 ± 0.01 dex kpc^{-1}; the reliability of this measurement being reflected in the small stan-

dard error. However, the magnitude of the gradient is critically dependent upon the status of the data-point for S 283-2. As discussed earlier, both C&N are enhanced in the atmosphere of this star – and hence, the photospheric abundances may not be representative of the progenitor ISM (see Smartt et al. 1996c). Exclusion of this data-point leads to a steeper gradient for nitrogen, viz. -0.09 ± 0.01 dex kpc^{-1}.

The majority of the remaining features that were observed in our spectra are transitions arising from multiplets 5 and 12 of N II. Therefore, we attempted to use this additional subset of lines to confirm the magnitude of the nitrogen abundance gradient. Excluding the data-point for S 283-2, the magnitude of the gradient (based on lines of multiplets 5 and 12) is in good agreement with that derived for the 3995 Å feature. Again, there is no evidence to suggest that the adoption of photometric and spectroscopic temperatures will introduce a bias, whilst using different treatments for the microturbulence parameter leads to a difference of less than 0.002 dex in the resultant gradients. Hence, given our concerns about the reliability of the S 283-2 data-point, we believe that a linear gradient of -0.09 ± 0.01 dex kpc^{-1} would better represent the variation of nitrogen in the Galactic disk.

4.7.3. Oxygen

The oxygen equivalent width dataset is the most extensive of the species observed in our spectra. Furthermore, the gradients that are derived are *not* critically dependent on any specific data-point. A gradient of -0.065 ± 0.010 dex kpc^{-1} is derived using the full dataset; furthermore, we find that adopting a subset of lines and stars improves the significance of the measured gradient, but does not significantly affect the magnitude.

Attempts were made to derive gradients using only those stars with photometric temperature determinations, and only those with spectroscopic determinations. However, only two data-points of oxygen abundances derived using photometric temperatures exist for Galactocentric distances greater than $R_g \sim 10$ kpc. No significant gradient was detected for this subset of stars which samples the Galactic disk over $R_g \sim 7$–10 kpc. However, we have previously highlighted the dangers involved with using spatially and statistically restricted samples of stars (Smartt & Rolleston 1997). Additionally, it may be that the metallicity is effectively constant across the $R_g \sim 7$–10 kpc region which covers the Local, Sagittarius and inner part of the Perseus arms (see Fitzsimmons et al. 1992 and Sect. 6.4).

Conversely, the analysis of clusters in the outer region ($R_g \sim 10$–17 kpc) utilizes mainly spectroscopic temperature indicators. However, several inner clusters were also analysed using this technique, and so stars with silicon ionization equilibrium temperatures are reasonably distributed across the Galactocentric range $R_g \sim 5$–17 kpc. The magnitude of the gradient using such a sub-sample (-0.066 ± 0.012 dex kpc^{-1}) is in excellent agreement with that derived using all the stars. This is not surprising, given that it is the lower metallicity objects found in the outer disk that mainly give rise to the oxygen gradient. However, the important point to note is that, oxygen abundances

derived using both photometric and spectroscopic temperatures were in excellent agreement for stars within the same cluster, and for clusters at similar R_g values. Further, those stars for which both Si III/Si IV and Strömgren indicators were available, the T_{eff} derived from each method was in good agreement (within the expected errors of ± 1000 K).

Hence, we conclude that our dataset will not be biased, even though stellar oxygen abundances have been derived using both photometric and spectroscopic temperature estimates, and that a linear gradient of -0.067 ± 0.008 dex kpc^{-1} best describes the current composition of the Galactic disk.

4.7.4. Magnesium

Our magnesium equivalent width dataset consists of only one feature, viz. the Mg II doublet at ~ 4481.2 Å; therefore our dataset, by definition, forms a homogeneous set of lines. It should be noted that for stars that display large projected rotational velocities, the Mg II 4481 Å feature can be blended with the nearby aluminium doublet (Al III 4479 Å); although, the latter feature generally makes a negligible contribution to the blended profile. However, those objects where the contribution from the aluminium line was estimated to be greater than 10% of the total equivalent width of the blend (less than 5% of our sample), were excluded from the analysis.

It was not possible to ascertain directly whether the adoption of both photometric and spectroscopic temperatures affected the derived value of the magnesium gradient. However, as for oxygen, there was good agreement between stellar abundance estimates deduced using different techniques within the same clusters, and between clusters at similar R_g values. Our data is best fitted with a gradient of -0.07 ± 0.01 dex kpc^{-1}.

4.7.5. Aluminium

The decrease in aluminium abundance as a function of increasing R_g is clearly observed (see Fig. 1); however, the extreme R_g data-point for S 283 is discrepant from this linear trend. For this latter object, the derived Al III abundance is slightly over-abundant as compared with the solar neighbourhood (see Smartt et al. 1996b). The α-elements (O, Mg, Si) for S 283-2 show consistent deficiencies relative to the solar neighbourhood – as would be expected, since these elements are believed to have a similar nucleosynthetic origin. However, it is unclear whether the derived aluminium abundance estimate for S 283-2 reliably reflects the present-day composition of the ISM at this position. Since this data-point is derived from one line in one star (and given the caveats described in Sect. 4.7.1), we have excluded it from the current analysis which has the purpose of estimating the linear decline of aluminium abundance with R_g. We shall return to this point in Sect. 6.3.

The full aluminium equivalent width dataset yields a gradient of magnitude -0.059 dex kpc^{-1}. This comprises observations of the 4479 Å doublet (which is not always resolved from the nearby and much stronger Mg II line at 4481 Å), the weak 4512 Å line which is poorly observed, and the 4528 Å doublet

which fulfills our selection criterion. Using a homogeneous set of lines (viz. Al III 4528 Å) for the homogeneous set of stars ($|T_{\mathrm{eff}} - T_{\mathrm{max}}| \leq 5\,000$ K), we deduce an abundance gradient of -0.050 ± 0.015 dex kpc^{-1}. This value does not appear to be biased by the inclusion of stars with different temperature indicators or by the adoption of 5 km s^{-1} for the microturbulence parameter.

4.7.6. Silicon

In early B-type stars, the three lines arising from the Si III multiplet at 4552–74 Å are moderately strong and are isolated – permitting the determination of reliable equivalent widths. These features were well observed in approximately 80% of our stellar sample, and thus form a homogeneous dataset. Our analysis shows a reasonably tight fit of the observed cluster abundances to a linear decline of -0.06 ± 0.01 dex kpc^{-1}. The magnitude of this gradient would appear to be unaffected by the adoption of different temperature indicators or a value of 5 km s^{-1} for the microturbulent velocity.

5. Non-LTE abundance analysis – verification of the LTE approach

5.1. Method of analysis

It is important to demonstrate that the assumption of LTE does not bias the derived abundance gradients, before we proceed to discuss our results in the context of other investigations. A full non-LTE analysis of our observational dataset would be a nontrivial task. This would involve the determination of non-LTE atmospheric parameters and non-LTE line formation calculations for approximately 80 stars and 6 species. The former is problematic, as the spectral data obtained at earlier epochs are no longer readily available (which would prevent the use of any profile fitting techniques). Also, McErlean et al. (1999) have shown that their non-LTE calculations (see Sect. 5.2.1) do not produce reliable results for some species. Furthermore, we do not believe that the amount of effort that would be required is commensurate with the additional information that maybe gained (see Sect. 5.2.3). We have therefore undertaken a non-LTE treatment of two species, viz. oxygen and magnesium, to test the validity of our LTE results. Lines of O II and Mg II possess the hottest and coolest peak line-strengths of the 6 species under consideration, and so, should illustrate the magnitude of non-LTE effects for our sample. Our approach is discussed in detail below.

5.1.1. Non-LTE model atmospheres

A grid of non-LTE model atmospheres, suitable for the analysis of main-sequence B-type stars, was generated using the code TLUSTY (Hubeny 1988). This grid covered an appropriate range in effective temperature ($20\,000 \leq T_{\mathrm{eff}} \leq 35\,000$ K) and included logarithmic gravities from $3.5 \leq \log g \leq 4.5$ dex. Models were calculated within the above parameter space at increments of 2 500 K and 0.25 dex in T_{eff} and $\log g$ respectively,

a microturbulence of 5 km s^{-1} and for two helium fractions $y = 0.09$ and $y = 0.20$. However, it should be noted that our entire stellar sample appeared to possess normal helium compositions (ie. $y = 0.09$).

The models, which contained only hydrogen and helium, assumed a plane-parallel geometry with both hydrostatic and radiative equilibrium. Non-LTE line-formation calculations were performed using the codes DETAIL (Giddings 1981) and SURFACE (Butler 1984). DETAIL calculates the level populations whilst allowing for departures from LTE, and SURFACE computes the emergent line profiles and fluxes. Computations were undertaken for the grid of model atmospheres described above, and a grid of element compositions corresponding to -1.2, -0.8, -0.4, 0.0 and $+0.4$ dex relative to solar for the two species O II and Mg II. Further details can be found in McErlean et al. (1999).

5.1.2. Non-LTE stellar atmospheric parameters

Element abundances were deduced by comparing our observed equivalent widths with the theoretical predictions generated using the above grid of non-LTE model atmospheres. However, the derived atmospheric parameters used in Sect. 3 were computed in LTE, and it is important that we adopt values appropriate to our non-LTE models. However, rather than estimating non-LTE effective temperatures/surface gravities for individual stars, we have derived a transformation between T_{eff}–$\log g$ points in the Kurucz LTE and non-LTE grids of model atmospheres. The temperature conversion was deduced from a comparison of the temperature–optical depth scales of the LTE and non-LTE models, for optical depths corresponding to that of the line-formation regions. This implied that for models with similar structures, the effective temperature label of the unblanketed non-LTE model was typically 1 500–2 500 K higher than that for the Kurucz line-blanketed model. We have adopted a temperature correction, ΔT, of $+2\,000$ K for LTE effective temperatures between 20 000–30 000 K and $\Delta T \sim +2\,500$ K for $30\,000 < T_{\mathrm{eff}}^{\mathrm{LTE}} \leq 32\,500$ K.

A gravity correction was derived by investigating the sensitivity of the Balmer line wings to non-LTE effects. Theoretical non-LTE hydrogen line profiles were generated using DETAIL/SURFACE for our grid of model atmospheres (see Sect. 5.1.1). These were compared with LTE hydrogen line profiles again generated using SURFACE for the same grid of model-atmospheres. A comparison of the LTE and non-LTE profiles at a particular temperature provides the corresponding non-LTE gravity correction. This effect was found to be negligible for non-LTE temperatures less than 30 000 K. However, for hotter temperatures our LTE computations overestimated the stellar surface gravity by up to 0.3 dex at $T_{\mathrm{eff}}^{\mathrm{NLTE}} \sim 35\,000$ K. Thus, we adopted a gravity correction of -0.1 dex for $30\,000 \leq T_{\mathrm{eff}}^{\mathrm{NLTE}} \leq 32\,000$ K and -0.2 dex for $32\,500 < T_{\mathrm{eff}}^{\mathrm{NLTE}} \leq 35\,000$ K. It should be noted that our findings for non-LTE gravity effects are similar to those of Mihalas & Auer (1970).

Hence, for our non-LTE analysis of the oxygen and magnesium line-spectra, we transformed our LTE atmospheric pa-
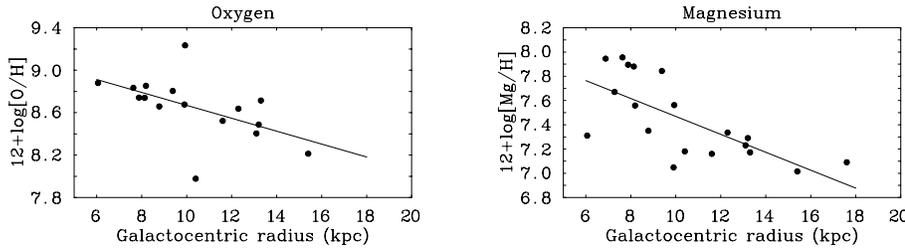
Fig. 2. Non-LTE oxygen and magnesium abundances determined for our homogeneous sample of B-type stars (*filled circles*). The solid lines represent a linear least-squares fit through the data points, the results of which are discussed in Sect. 5.2.

rameters (see Sect. 4) into appropriate non-LTE (T_{eff}, $\log g$) pairs by applying the temperature and gravity corrections described above. This type of transformation assumes that the temperature and gravity corrections are orthogonal. Given the relatively small magnitudes of the non-LTE corrections, any non-orthogonal effects should be much smaller than the observational uncertainties associated with the determination of the atmospheric parameters (viz. $\Delta T \sim 1\,000$ K and $\Delta \log g \sim 0.2$ dex). This also justifies our use of 'step-like' temperature/gravity corrections as opposed to graduated transformations. A value of 5 km s^{-1} for the microturbulent velocity was adopted for all stars in the subsequent non-LTE analysis. This has been found previously to be appropriate for main-sequence B-type stars by Gies & Lambert (1992). Indeed, our tests showed that values of ξ derived using the O II line spectra were very similar in LTE and non-LTE.

5.1.3. Homogeneous subsets of lines/stars

Our LTE analysis demonstrated that it was possible to identify homogeneous sub-samples of stars for each species (see Sect. 4.3). Hence, we have adopted similar homogeneous subsets of stars in the non-LTE analysis. For O II, stars were selected with effective temperatures within $\pm 5\,000$ K from the peak line-strength of the species which corresponds to 29 500 K in non-LTE. However, the Mg II spectrum has a peak line-strength that is much cooler than any of our stellar sample; thus, we considered objects within $\pm 5\,000$ K of the mean effective temperature of the stellar sample, viz. $\overline{T_{\text{eff}}} \sim 27\,000$ K for the non-LTE models.

In Sect. 4.2, we identified homogeneous subsets of lines for each species, with which the LTE abundance analysis was undertaken. However, it was not possible to model all of these transitions within SURFACE/DETAIL. Thus, we have performed a non-LTE analysis using a homogeneous subset of 9 oxygen lines (O II 4072.16, 4078.84, 4092.93, 4132.80, 4590.97, 4596.18, 4638.86, 4661.63, 4676.24 Å) and the magnesium doublet (Mg II 4481.23 Å).

5.2. Non-LTE results

5.2.1. Oxygen

The non-LTE analysis of the O II line-spectra yielded an abundance gradient of -0.061 ± 0.005 dex kpc^{-1}. The mean cluster, oxygen abundances are tightly distributed around the least squares fit, with only two points deviating by more than 0.2 dex

(see Fig. 2). One of these data-points represents the mean oxygen abundance derived for the isolated field star RLWT-41 which was noted by Smartt et al. (1996b, 1996a) to currently lie in the inter-arm gap between the Local and the Perseus spiral arms. Given its very low metallicity for a Galactocentric distance of 10 kpc, it may have formed in situ between the spiral arms. The second data-point that is discrepant represents the mean oxygen abundance as determined from 5 stars in the open cluster $h + \chi$ Per. This is a well observed cluster in the Perseus spiral arm and should be representative of the solar neighbourhood. Hence, at first inspection, it is not obvious why the oxygen abundance is so discrepant from the linear decline observed for the Galaxy. However, our LTE analysis revealed that 3 of the $h + \chi$ Per stars are indeed evolving off the main-sequence, and we measured larger values (12 km s^{-1}) for their microturbulent velocity. Adopting a value of 5 km s^{-1} for this parameter in the non-LTE analysis may lead to an overestimation of the cluster oxygen abundance.

Comparison of the LTE and non-LTE oxygen gradients provides encouraging agreement. However, it is important to consider possible sources of inhomogeneities between the two datasets. First, the dataset of lines used in these analyses are different. Secondly, the non-LTE line-formation calculations for O II were not reliable for $T_{\text{eff}}^{\text{NLTE}} > 30\,000$ K; a consequence of the model-atmosphere codes (DETAIL/SURFACE) inadequately modelling the O III ion. Hence, we re-analysed the O II dataset in LTE using the same subset of lines/stars as used in the non-LTE analysis (see Sect. 5.1.3). The result is very encouraging with the revised LTE analysis yielding a gradient of -0.061 ± 0.006 dex kpc^{-1}, in excellent agreement with the non-LTE result.

5.2.2. Magnesium

The non-LTE analysis of the Mg II ion did not suffer from the complexities associated with the O II ion. The observational dataset consists of the Mg II 4481.23 Å transition, and this was reliably modelled in both LTE and non-LTE for the same homogeneous sub-sample of stars. Thus, the results can be directly compared. The non-LTE analysis yields a gradient of -0.074 ± 0.010 dex kpc^{-1}, again in excellent agreement with our LTE investigation (viz. -0.073 ± 0.012 dex kpc^{-1}).

5.2.3. Conclusions

It is not surprising that abundance gradients derived for oxygen and magnesium using LTE and non-LTE techniques do not differ

significantly. First, it has been accepted for some time that LTE is a reasonable assumption when analyzing the spectra of main-sequence B-type stars (Hardorp & Scholz 1970; Peters 1976). Secondly, non-LTE effects in such a temperature and gravity regime have been found previously to be relatively small for the 6 species under consideration (see, for example, Becker & Butler 1988, 1989, 1990). Thirdly, by using sub-samples of stars with similar effective temperatures, our approach is essentially a differential treatment, which should minimize the effects of such systematic errors. Thus, we conclude that the LTE analysis should be reliable for estimating the magnitude of the metal abundance gradients in the present-day Galactic disk; although, we recognize that the absolute abundance values at any particular Galactocentric distance may be in error. In the subsequent discussion (see Sect. 6), we have adopted the results of the LTE analysis.

6. The nature of the observed Galactic abundance gradient

6.1. A comparison with previous B-star studies

Smartt & Rolleston (1997) were the first to report the detection of a significant Galactic abundance gradient using young, early-type stars. In this current paper, we have utilized the same dataset of clusters with the addition of NGC 457; furthermore, we have comprehensively examined the significance of adopting homogeneous subsets of lines and stars. In summary, this study is in excellent agreement with the results of Smartt & Rolleston, and internal agreement is found between the non-LTE and LTE treatments. This suggests that it is not the chosen methodology which is important, for example, a full LTE treatment (Sect. 4), a full non-LTE treatment (Sect. 5), or a combination of LTE line-blanketed model-atmospheres and non-LTE line formation calculations (Smartt & Rolleston 1997, Gummersbach et al. 1998), but that a consistent approach must be used to derive abundance estimates in a homogeneous stellar dataset.

More recently, Gummersbach et al. (1998) determined abundance gradients for C, N, O, Mg, Al and Si using a sample of 16 early-B main-sequence stars at Galactocentric distances of $R_g \sim 5$–14 kpc. This study entailed a re-analysis and an extension of the observations of Kaufer et al. (1994) towards the Galactic centre. In general, their results are in good agreement with our study – yielding a mean, light element, abundance gradient of -0.07 dex kpc^{-1}. However, Gummersbach et al. (1998) ascribe the fact that they now determine significant abundance gradients (cf. Kaufer et al. 1994, Kilian-Montenbruck et al. 1994) to their use of a sub-solar metallicity model-atmosphere. We dispute that this is the real reason for the derivation of a steep gradient. For example, our tests have shown that the assumption of a normal, Galactic Population I chemical composition do not lead to significant errors in the resultant model-atmosphere analyses of B-type stars in the Magellanic system, where metal deficiencies are upto 0.8 dex (see Dufton et al. 1990b, Rolleston et al. 1999). The arguments forwarded by Gummersbach et al. (1998) tend to imply that it is not possible to reliably study such metal-poor stars – unless an appropriate metallicity model-atmosphere is adopted. However, previous work on metal-poor,

hot stars has not required such an approach in order to determine valid stellar abundances (see Lennon et al. 1996, Venn 1999).

In order to demonstrate the validity of our methods, we considered one of the most metal deficient stars in our sample, viz. S 289-2 which has a Galactocentric distance of 15.4 kpc and a mean metallicity of approximately -0.5 dex relative to the solar neighbourhood. Stellar atmospheric parameters were derived using the Si III/Si IV ionization balance and the hydrogen line profiles for both a normal metallicity, LTE model-atmosphere ($T_{\rm eff} = 28\,500$ K; $\log g = 4.0$ dex; $\Delta[X/H] = 0.0$ dex) and a reduced metallicity model-atmosphere ($T_{\rm eff} = 29\,000$ K; $\log g = 4.0$ dex; $\Delta[X/H] = -0.5$ dex). We note that (as expected) the temperature-optical depth scales are very similar for both models, while the higher effective temperature label in the latter case probably reflects the decrease in line-blocking. An abundance analysis was subsequently undertaken using both models, and excellent agreement (to within 0.03 dex) was found between the two sets of abundance estimates for all species. Hence, we re-iterate that this effect is negligible for the metallicity regime that is encountered in the outer Galactic disk.

Moreover, a direct comparison with the work of Kaufer et al. (1994) is not valid. First, this investigation combined their own B-star abundance estimates with azimuthally averaged values taken from previously published work in the literature. Their derivation of a shallow (or non-existent) gradient illustrates the dangers of using an inhomogeneous dataset, where abundance estimates have been determined using different model-atmosphere codes, atomic data/model atoms and techniques. Secondly, Kaufer et al. (1994) adopted incorrect abundances or distances for two outer disk objects, viz. Dolidze 25 and S 208-6 (see Smartt & Rolleston 1997 for further details).

It should be noted that we do not dispute the magnitude of the gradients found by Gummersbach et al. (1998), nor their methodology, but rather their explanation for the failure of previous investigations to detect such gradients. Indeed, both investigations derive an oxygen gradient of -0.067 ± 0.008 dex kpc^{-1}. Such excellent agreement is probably not surprising, given the plethora of O II lines observed in the spectra of early B-type stars, and the fact that a consistent approach was used within each study. Gradients deduced for nitrogen, magnesium and aluminium are also found to be in agreement (within the errors of measurement). Hence, the shallower gradient found by both studies for aluminium may be a real effect in the Galactic disk. On the other hand, significant differences exist between our estimates of the Galactic abundance gradients for carbon and silicon (see Table 4) and those presented by Gummersbach et al. (1998). Our estimate of a carbon gradient is -0.07 ± 0.02 dex kpc^{-1}; in good agreement with that found for nitrogen and the α–elements. Gummersbach et al. deduce a much shallower gradient, viz. -0.035 ± 0.014 dex kpc^{-1}. For silicon, our data is fitted by a slope of -0.06 ± 0.01 dex kpc^{-1} which is consistent with our results for oxygen and magnesium; in contrast to Gummersbach et al., who measure a much steeper decline of -0.11 ± 0.03 dex kpc^{-1}. One would expect a correlation between the gradients deduced for O–Mg–Si, as these α–elements

possess similar nucleosynthetic origins. Gummersbach et al. do not comment on their apparent lack of correlation.

6.2. A comparison with Galactic nebular studies

It is also interesting to compare our results with those found from nebular studies and, in particular, of other young objects such as H II regions. The only elements in common between these latter investigations and our study are nitrogen and oxygen.

Nitrogen: Shaver et al. (1983) deduced a nitrogen gradient of -0.090 ± 0.015 dex kpc^{-1} from a study of 67 H II regions spanning the range $3.5 \leq R_g \leq 14.0$ kpc. More recently, Afflerbach et al. (1997) derived a value of -0.072 ± 0.006 dex kpc^{-1} from the [N III] 57 μm lines in 18 H II regions with Galactocentric distances between $R_g \sim 0 - 12$ kpc. By comparison, studies of older planetary nebulae have yielded a slightly smaller gradient of -0.05 dex kpc^{-1} (Pasquali & Perinotto 1993).

Oxygen: This element was also studied by Shaver et al. (1983) and Afflerbach et al. (1997) who deduced an oxygen abundance gradient of -0.070 ± 0.015 dex kpc^{-1} and -0.064 ± 0.009 dex kpc^{-1} respectively. In a study of disk planetary nebulae, Maciel & Quireza (1999) reported an oxygen gradient of -0.06 dex kpc^{-1}.

Comparison of our results for young, B-type stars with analyses of H II regions demonstrate excellent agreement (for at least those elements in common, viz. nitrogen and oxygen). Thus, it would appear that the discrepancies between earlier sets of investigations have been resolved, and that abundance gradients of -0.09 dex (nitrogen) and -0.065 dex (oxygen) are appropriate for young objects in the Galactic disk.

6.3. The peculiarity of the distant star S283-2

There is an apparent correlation between the individual α-elements (O, Mg, Si) and between N & Al within the atmosphere of S 283-2. The former group are all deficient by similar amounts relative to objects in the solar neighbourhood. This is not surprising since they possess a similar nucleosynthetic origin; α-elements are believed to be predominantly produced in the violent deaths of massive stars (ie. Type II supernovae). We note that our stellar oxygen abundance is in excellent agreement with the gas phase abundance of 8.2 dex as determined by Vílchez & Esteban (1996) for the S 283 H II region. The dominant source of nitrogen in the ISM is still a matter of debate. It is thought that intermediate mass stars ($4M_\odot \lesssim M \lesssim 8M_\odot$) produce primary nitrogen through dredge-up episodes in the course of their evolution (Renzini & Voli 1981), with secondary nitrogen production occuring in stars with a wide range of masses. Such mixing processes for primary nitrogen production are accompanied by continuous mass loss via a stellar wind on the red giant branch (RGB) and asymptotic giant branch (AGB), and the expulsion of a significant fraction of the remaining mass in the form of a planetary nebula. We find a higher nitrogen com-

position for S 283-2 (7.65±0.30 dex) compared to the nebular studies of Vílchez & Esteban (1996) and Fich & Silkey (1991), viz. ∼7.2 dex.

It is interesting to note that we also find the abundance estimate derived for aluminium to be enhanced (relative to the underlying O-Mg-Si values) in the atmosphere of S 283-2 – similar to the behaviour of C & N. Correlations have been observed for CN–Na and CN–Al in the atmospheres of globular cluster red giants (see, for example, Kraft et al. 1997). These correlations have been explained by very deep mixing, which would produce nitrogen and sodium overabundances and, perhaps, somewhat smaller aluminium enhancements (via proton capture processes). Hence, our observed correlation between the enhancements of Al and C&N in the atmosphere of S 283-2 may be causal. For example, if the photospheric abundances are representative of the present-day metal-content of the ISM, this could be indicative of an initial mass function (IMF) in the outer Galactic disk that was biased towards intermediate mass stars relative to high mass stars (which are the dominant source of α-elements). However, the observed IMF appears approximately constant over a range of environments within the Local Universe – and there is no reason to believe that the outer Galactic disk is any different. Indeed, these correlations are only found in one star in one H II region and given the possible problems with the observational data as discussed in Sect. 4.7.1, we cannot draw any firm conclusions from our abundance results. Further, the aluminium enhancement is greater than that found for C&N, and there is no other evidence for a flattening of the C, N or Al abundance gradients at $R_g > 15$ kpc.

6.4. Linear relationship vs step function decline in metallicity

In our discussion so far, we have implicitly assumed that the Galactic abundance gradients can be described by a linear decline in metallicity with increasing values of R_g. Recently, Twarog et al. (1997) challenged the validity of this assumption. Using a sample of 76 open clusters, they derived [Fe/H] abundances based on DDO photometry and/or moderate dispersion spectroscopy. They concluded that a significant change in metallicity does occur over the Galactocentric range, $6.5 \leq R_g \leq 15$ kpc, but rather than a linear transition with distance, Twarog et al. (1997) interpreted their results as being consistent with a relatively abrupt discontinuity in the metallicity of the Galactic disk near $R_g = 10$ kpc. Their data provided observational evidence for two distinct groups of clusters; an inner group between $R_g = 6$–10 kpc and an outer group between $R_g = 10$–15 kpc, with the latter group being ∼0.3 dex more metal deficient than the former. Furthermore, the metallicity gradient within each group was weak to non-existent. Twarog et al. (1997) argue that previous samples were inadequate to elucidate the precise nature of such sub-structure within the Galactic disk; given the significant scatter between the data-points, the step function was effectively smeared into a linear gradient. Thus for example, Janes (1979) who made a tentative detection of such a feature in the past – interpreted it as a steepening of the gradient rather than a discontinuity. It should be noted that

the open cluster dataset (ages $\sim$10 Myr–10 Gyr) of Twarog et al. (1997) sample quite different epochs compared to the young stars and H II regions that we have discussed. Hence, an age-metallicity relationship may also confuse any comparisons, as well as the fact that the elements we have presented have totally different origins to iron, the bulk of which is synthesized in low mass SN Type I supernovae.

Simpson et al. (1995) also suggested that their H II region abundances (of nitrogen and sulphur) derived from far-IR observations may be better fit with a step function rather than a linear gradient; however, their results could not definitively discriminate between the two cases. The discontinuity occurred at a Galactocentric distance of approximately 6 kpc with a difference of $\sim$0.6 dex between the mean metallicity level of the two zones (within $0 \leq R_{\mathrm{g}} \leq 10.5$ kpc). Rudolph et al. (1997) presented inconclusive evidence of a two step function for the log N/O gradient over $0 \leq R_{\mathrm{g}} \leq 17$ kpc. On the other hand, Afflerbach et al. (1997) contest that a step function fits the abundance data within the inner 10 kpc of the Galactic disk; they find linear gradients of approximately -0.07 dex kpc^{-1} for nitrogen, oxygen and sulphur from the study of 34 compact H II regions with $R_{\mathrm{g}} \sim$ 0–12 kpc. Vílchez & Esteban (1996) concluded that although the metallicities of outer disk H II regions are significantly below solar, the gradient in this part of the Galaxy may be relatively flat – which is further evidence of a two-tier relation. Smartt (2000) has presented a full review of these H II region, PN and B-star studies, and concludes that there is no strong evidence against the simple linear form of the Galactic abundance gradient.

We have inspected our homogeneous dataset of metal abundances, over the Galactocentric range 6–18 kpc, to see if there is any evidence for a step function. Such a conclusion could perhaps explain why Fitzsimmons et al. (1990; 1992) found no systematic abundance variations – as these studies extensively surveyed the region within $\sim$2 kpc from the Sun, but failed to sample sufficiently the outer disk beyond the Perseus spiral arm ($R_{\mathrm{g}} \sim$ 11 kpc). Furthermore, Twarog et al. (1997) suggested that our oxygen dataset presented by Smartt & Rolleston (1997) provides evidence for their alternative interpretation. The 11 clusters and associations between $R_{\mathrm{g}} \sim$ 6–10 kpc exhibit no gradient at all. The entire source of the gradient is provided by the oxygen abundance estimates for the 10 clusters/associations in the outer disk ($R_{\mathrm{g}} > 11$ kpc). The latter group exhibit oxygen compositions approximately 0.5 dex lower than the clusters/associations in the solar neighbourhood.

As Twarog et al. (1997) concluded that there was evidence for a metallicity discontinuity in the Galactic ISM around $R_{\mathrm{g}} \sim 10$ kpc, we have followed their approach by estimating abundance gradients within an inner ($R_{\mathrm{g}} < 10.5$ kpc) and outer zone ($R_{\mathrm{g}} > 10.5$ kpc). The results are tabulated in Table 5 and discussed below.

Carbon: there is no evidence to suggest that a two-zone model would be more appropriate for this element. However, the carbon dataset is much smaller than that obtained for other species.

Table 5. Results for the two-zone model.

Element	$d[X/H]dR_{\mathrm{g}}$ (dex kpc^{-1})		
	$R_{\mathrm{g}} < 10.5$ kpc	$R_{\mathrm{g}} > 10.5$ kpc	Full dataset
C	-0.06 ± 0.05	-0.04 ± 0.04	-0.07 ± 0.02
N	-0.04 ± 0.04	-0.09 ± 0.08	-0.09 ± 0.01
O	-0.02 ± 0.01	-0.10 ± 0.05	-0.067 ± 0.008
Mg	-0.13 ± 0.03	-0.03 ± 0.02	-0.07 ± 0.01
Al	-0.02 ± 0.04	$+0.05 \pm 0.04$	-0.050 ± 0.015
Si	-0.06 ± 0.04	-0.06 ± 0.05	-0.06 ± 0.01

Nitrogen: the scatter in the abundance estimates is relatively large ($\sim$0.25 dex) at any particular R_{g}. Again, there is no evidence to suggest that a two-zone model would be more appropriate. However, the slope of the gradient within the outer zone is critically dependent on the data-point for S 283-2 which we excluded from our analysis (see Sect. 4.7.2). Inclusion of the abundance estimate for this object would lead to a much flatter gradient ($+0.01$ dex kpc^{-1}) in the outer zone.

Oxygen: this metal-line spectrum represents the most extensive in our sample. The LTE results presented in Fig. 1 clearly show that a gradient is small or absent in the inner ($R_{\mathrm{g}} < 10.5$ kpc) region; in contrast, the abundance estimates for clusters in the outer disk decline by approximately -0.1 dex kpc^{-1}. It is interesting to note that the non-LTE analysis provides a significantly larger coefficient of determination than the LTE least-squares fit. Furthermore, in non-LTE both regions exhibit comparable oxygen gradients (see Fig. 2) to that obtained for clusters over the entire Galactocentric range. It is possible that small non-LTE effects may be sufficient to explain the lack of an observed gradient in the inner ($6.0 \leq R_{\mathrm{g}} \leq 10.5$ kpc) region. However, we find that the gradients are often ill-defined within each zone, with their magnitudes being critically dependent upon the end data-points. This is a consequence of the small number of data-points within each zone which also covers a small range of Galactocentric distances, and the observed scatter in metallicity at any one particular Galactocentric radius (see, for example, Edvardsson et al. 1993).

Magnesium: no significant gradient was detected in the outer disk. This contrasts with a steep decline in metallicity observed for $R_{\mathrm{g}} < 10.5$ kpc, although the measured spread in the abundances in this region is as large as 0.35 dex.

Aluminium: a shallow gradient may be present in the inner zone; however, the positive gradient observed in the outer region is skewed by the data-point for S-289.

Silicon: like oxygen, the silicon line spectrum is well observed. In both zones, the least-squares fits to the data yield gradients that are comparable to that deduced using the complete dataset.

Given our comments for the best observed species (viz. oxygen and silicon), we do not believe that it would be better to fit

our data with a two-zone model. Indeed, to definitively test the conclusions of Twarog et al. (1997) using observations of B-type stars, abundance information would be required for many more clusters.

7. Discussion: abundance ratios in the disk and chemical evolution

7.1. Chemical evolution models

Portinari & Chiosi (1999) have recently presented new chemical evolution models of the Galactic disk. They investigated the dependence of disk evolution upon the star formation rate (SFR), as a function of both the total surface mass density and the surface gas density. Star formation, and the subsequent stellar wind outflow and supernovae explosions, tends to support the surrounding gas against further gravitational contraction; hence, star formation becomes a self-regulating process. Using the star formation law of Dopita & Ryder (1994) which incorporates this type of self-regulation, Portinari & Chiosi (1999) have been able to reproduce the radial oxygen variations (viz. a gradient of -0.07 dex kpc^{-1}). However, these models require the infall of gas to have occurred at a greater rate in the inner regions during the formation of the Galactic disk. Simulations of this "inside-out formation" scenario also predict that the radial abundance profile within $R_g \sim 8$ kpc should flatten, approximately 15 Gyr after the formation of the Galaxy. However, these models can not simultaneously reproduce the oxygen abundance gradient and radial gas distribution. With further development of dynamical models incorporating radial gas flows, Portinari & Chiosi (2000) have been able to also reproduce the magnitude of the oxygen abundance gradient *without* having to assume the inside-out formation model of the Galaxy. Unfortunately, it is not possible to distinguish between these two evolution scenarios at present using the current set of element abundance gradients. However, the latter model (incorporating radial flows) is slightly favoured as it reproduces the gas distribution and the presence of the 4 kpc molecular ring.

7.2. Abundance ratios

In Fig. 3 we have plotted the logarithmic abundance ratios of Mg/O and Si/O as a function of Galactocentric radius. The ratios were calculated using the element abundance estimates presented in Table 3, and in each case, a least-squares straight line fit to the data-points indicate a flat relation. Indeed, this is not surprising as similar O-Mg-Si correlations are observed in the Magellanic Clouds (Rolleston et al. 1993b, 1996) and M33 (Monteverde et al. 2000). Furthermore, the observed correlation of Si and Mg with O (Fig. 3) provides firm evidence that they are all primary elements, produced during ^{12}C and subsequent ^{16}O burning in pre-supernova ($M \gtrsim 10 M_\odot$) massive stars (see Arnett 1996; Matteucci & Francois 1989).

It is more interesting to compare the abundance ratios of elements which are predicted to be formed in distinctly different nucleosynthetic sites and during different phases of stellar evolution. In Fig. 4a, we show our estimates of the logarithmic N/O
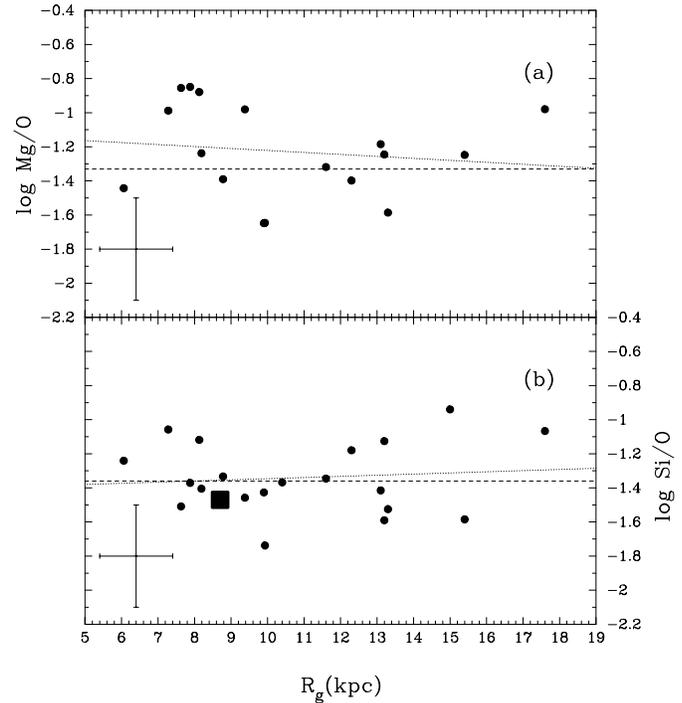

Fig. 3a and b. Plotted here are **a** log Mg/O and **b** log Si/O versus Galactocentric radius (R_g) for each of our clusters (filled circles). Ratios were determined using the abundance estimates listed in Table 3. The solid square symbols are the non-LTE oxygen and silicon values derived from B-stars in Orion (Cunha & Lambert 1994), and the dashed lines are the solar ratios from Grevesse & Noels (1993). Typical error bars are shown in each frame. The least-squares fits to our data-points are shown as dotted lines. Their values of -0.01 ± 0.02 and 0.007 ± 0.02 dex kpc^{-1} respectively imply flat gradients within the errors.

ratio as a function of Galactocentric radius. We derive a gradient for log N/O of -0.04 ± 0.02 dex kpc^{-1}, implying that in the outer Galactic disk ($R_g \sim 16$–18 kpc), the N/O ratio is $\sim$40% of the solar value. Rudolph et al. (1997) have also measured N/O ratios in H II regions with $R_g = 0$–17 kpc. While they observe a decreasing trend of N/O with increasing R_g, Rudolph et al. claim that their data is better fit with a step function. We have applied a least-squares fit to their (log N/O, R_g) data-points, and derive a gradient of -0.03 ± 0.01 dex kpc^{-1}, in good agreement with our stellar data.

Vila-Costas & Edmunds (1993) observed a proportional decrease of log N/O with decreasing log O/H (or increasing R_g) in a large sample of spiral galaxies, for metallicities greater than that corresponding to an oxygen abundance of $12 + \log[O/H] \sim 8.3$ dex. They proposed that the dominant source of nitrogen at such metallicities was secondary production, ie. synthesized from C and O seed nuclei of the progenitor interstellar material through the CNO-cycle in a range of stellar masses. In such a regime, primary nitrogen production makes a minimal contribution, and the simple closed-box models of Vila-Costas & Edmunds reproduce the observed evolution of the N/O gradi-
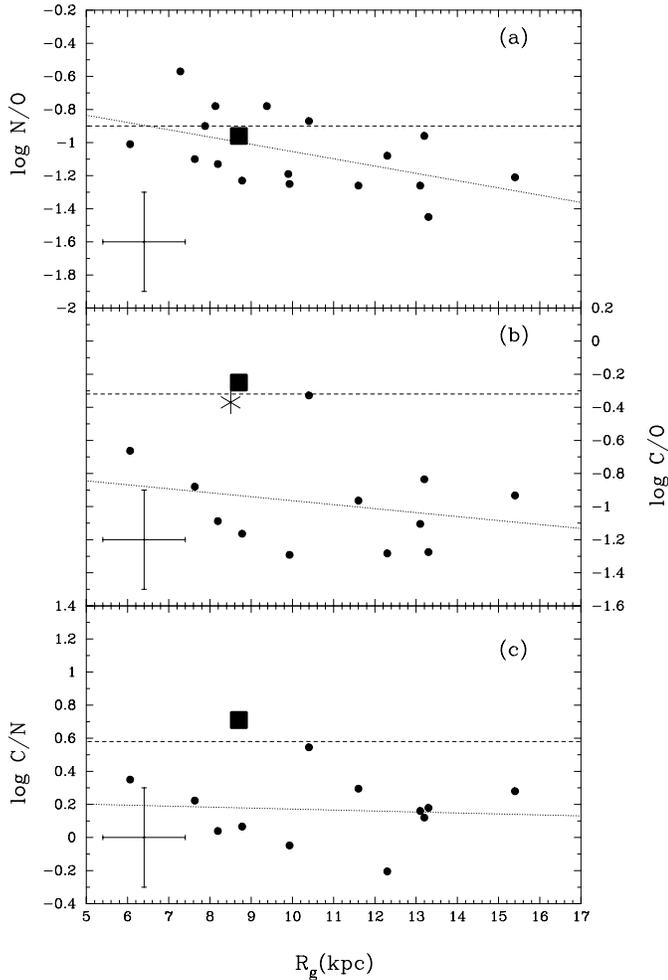
Fig. 4a–c. Plotted here are **a** log N/O, **b** log C/O and **c** log C/N versus Galactocentric radius (R_g) for each of our clusters (filled circles). Ratios were determined using the abundance estimates listed in Table 3. The solid square symbols are the non-LTE B-star values for Orion (Cunha & Lambert 1994); the star symbol represents the gas-phase values of the Local ISM (Meyer et al. 1998, Sofia et al. 1997); and the dashed lines are the solar ratios from Grevesse & Noels (1993). Typical error bars are shown in each frame. The least-squares fits to our data-points of -0.04 ± 0.02, -0.02 ± 0.03 and -0.01 ± 0.02 dex kpc^{-1} for plot **a–c** respectively are shown as the dotted lines.

ent. By contrast, at low metallicities ($12 + \log[\text{O/H}] \leq 8.0$ dex) secondary nitrogen production becomes less significant (due to its inherent dependence on metallicity), and a break in the N/O gradient is predicted. Our estimates of the N/O ratio and oxygen abundance in the outer Galactic disk (viz. $\log \text{N/O} \simeq -1.3$ dex at $\log \text{O/H} \simeq 8.3$ dex) are quantitatively consistent with the linear dependence observed by Vila-Costas & Edmunds in early-type spirals (assuming a Sbc type for the Milky Way; de Vaucouleurs & Pence 1978). Hence, it would appear that secondary production dominates the evolution of N in the Galactic disk out to approximately 17 kpc.

We note that our results are in reasonable agreement with the N/O variation observed in NGC 2403 (Garnett et al. 1997),

but that M33 and M81 (Vílchez et al. 1988; Henry & Howard 1995) exhibit much shallower gradients. By contrast, Henry & Howard (1995) find a markedly steeper gradient of N/O in M101. Advances in modern instrumentation warrants a more detailed study of external galaxies to improve the global compilation of Vila-Costas & Edmunds (1993).

It is possible that some B-stars in our sample may show photospheric nitrogen abundances which are not representative of the progenitor material. Evolutionary models suggest that turbulent diffuse mixing in the radiative envelope of massive stars may cause some core processed material to be mixed to the surface (eg. Dennissenkov 1994; Fliegner et al. 1996). Photospheric nitrogen enhancements are to be expected, accompanied by carbon deficiencies (as it is mainly C which is converted to N in the CNO-cycle), but whether or not this is a common occurrence in massive stars is still controversial (Gies & Lambert 1992, Venn 1999). We find no evidence of an anti-correlation between C and N (see Fig. 4c and Hibbens et al. 1998); hence, we believe our discovery of a significant N/O variation within the Galactic disk, open clusters to be real, in good agreement with nebular studies of external galaxies.

While the Triple Alpha reaction is believed to be the nuclear process responsible for the production of C nuclei, the major source (or stellar mass range) which contributes carbon to the ISM is still rather uncertain (see Garnett et al. 1999; Gustafsson et al. 1999). Recent work on HST-UV spectra of H II regions in M101 and NGC 2403 (Garnett et al. 1999) indicates that the C/O ratio may show a gradient of approximately -0.1 to -0.2 dex scalelength^{-1}. However, the observations consisted of only 3 data-points per galaxy. Furthermore, their abundance calculations/analysis were critically dependent upon two factors, viz. 1) the determination of a correction factor for the internal galactic reddening, and 2) the unobserved amounts of carbon that have depleted onto grains. The observed gradient in C/O may be explained if the stellar winds of massive stars play an important role in the yields of both C and O. Metallicity dependent yields, whereby C production increases with metallicity at a greater rate than O production, have been suggested previously by Maeder (1992). In Fig. 4b, we plot the logarithmic C/O ratio as a function of Galactocentric distance. Unfortunately, due to the large scatter in the individual estimates of the C/O ratio, it is not possible to conclude whether our dataset supports the findings of Garnett et al. (1999). We note that our absolute values of the $\log$ C/O ratios are significantly offset from the Orion and solar values – see Fig. 4b. This may be possibly the result of our absolute LTE C & O abundances being in error, and the line-strengths of the carbon and oxygen line-spectra peaking at different temperatures. However, this should not prevent the detection of any significant trends in the C/O ratio. In any case, we recommend that a more extensive study be undertaken using the red C II lines and non-LTE techniques, in order to investigate the C/O relationship in the Galactic disk. Finally, we note that the $\log$ C/N variation shown in Fig. 4c appears flat, within the relatively large uncertainties, which is also consistent with that found for M101 and NGC 2403.
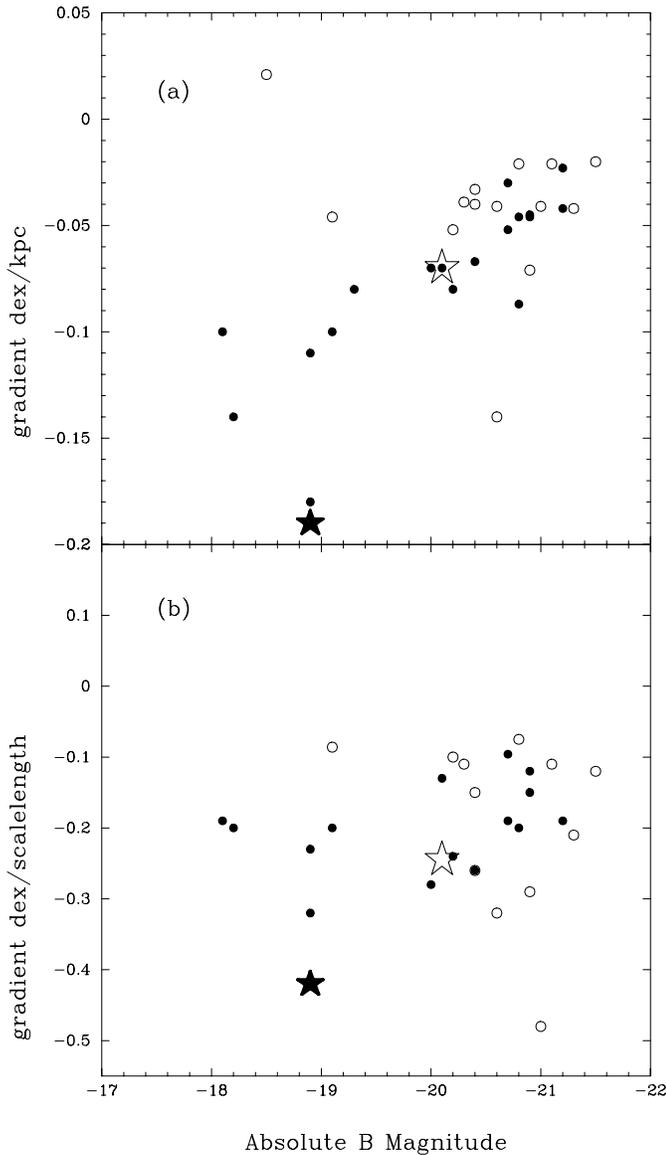
then the steepness of the abundance gradient (in real physical terms) is closely constrained by the mass of the galaxy. Clearly, future evolutionary models of spiral galaxy formation and evolution need to take account of this observed correlation. In order to put our results of the Milky Way into context, we have reproduced the figure of Garnett et al. in Fig. 5. This demonstrates that the Milky Way sits along the normal sequence in both the plots, indicating its chemical history has been reasonably normal in the context of other spirals, given its mass. However, in order to elucidate the mechanism responsible for creating radial abundance gradients and the apparently homologous evolution of our Galaxy and other similar spirals – new models will need to incorporate the observed correlations between such global properties as discussed, for example, by Garnett et al.

8. Conclusions

1. The abundance analyses are based on an extensive observational dataset comprising high-resolution spectroscopy of 80 B-type main-sequence stars in 19 Galactic, young open clusters/associations distributed over $6 \leq R_{\rm g} \leq 18$ kpc.
2. Using homogeneous subsets of stars and lines, we deduce significant abundance gradients for C, N, O, Mg, Al & Si. We conclude that the radial distribution of light elements in the Galactic disk can be represented by a linear gradient of -0.07 ± 0.01 dex kpc^{-1}, with a steeper gradient being more appropriate for nitrogen, viz. -0.09 ± 0.01 dex kpc^{-1}.
3. Abundance gradients derived for oxygen and magnesium using LTE and non-LTE model-atmosphere techniques do not differ significantly. Thus, we conclude that the LTE analysis should be reliable for estimating the magnitude of the metal abundance gradients in the present-day Galactic disk.
4. Comparison of our nitrogen and oxygen gradients for young, B-type stars are in excellent agreement with the analyses of H II regions. Thus, it would appear that the discrepancies between earlier sets of investigations have been resolved. Several factors have almost certainly contributed to the failure of detecting significant abundance gradients in the past, viz. the use of inhomogeneous datasets, and/or the use of small samples of objects with a restricted range of Galactocentric distances.
5. Twarog et al. (1997) report evidence of an abrupt discontinuity in the metallicity of the Galactic disk at $R_{\rm g} \sim 10$ kpc. However, we do not believe that our abundance estimates of B-type stars in young, open clusters would be better fitted with a two-zone model.
6. The variation of O-Mg-Si as a function of Galactocentric distance are well correlated; further evidence that these elements have a similar nucleosynthetic origin. On the other hand, the $\log$ N/O ratio displays a linear decline of -0.04 ± 0.02 dex kpc^{-1} with $R_{\rm g}$. This result is in good agreement with that found for H II regions in the Milky Way (Rudolph et al. 1997) and external spiral galaxies (see Vila-Costas & Edmunds 1993). Our results suggest that secondary nitrogen production (cf. primary production) is dominant in the Galactic disk out to ~ 17 kpc.

Fig. 5a and b. The compilation of Garnett et al. (1997) showing the abundance gradients for a selection of local spiral galaxies in terms of **a** physical units and **b** scalelengths, both as a function of M_B. The filled and open circles represent non-barred spiral galaxies and 'mixed' types respectively. The Milky Way is shown as the large open star with $M_B = -20.1$ and R(scale) = 3.5 kpc (de Vaucouleurs & Pence 1978). We also show the stellar abundance gradient in M33 as derived by Monteverde et al. (2000) as the large filled star.

7.3. The Milky Way as a normal spiral galaxy

Garnett et al. (1997) and Skillman (1998) have highlighted that there is a remarkable correlation between the magnitude of the oxygen abundance gradient (in dex kpc^{-1}) in spiral galaxies and the galaxy luminosity (as measured by M_B), with the truely non-barred spirals displaying a tighter relationship with less scatter. However, no such correlation is found when the abundance gradient is expressed in terms of dex per disk scalelength. If the mass-to-light (M/L) ratios are similar in these galaxies,

7. Garnett et al. (1997) have demonstrated that there is a remarkable correlation between the abundance gradient and the luminosity of a spiral galaxy. Comparison of our results for the Milky way with this relationship, suggests that our Galaxy has had a reasonably normal chemical history, given its mass.

References

Afflerbach A., Churchwell E., Accord J.M., et al., 1996, ApJS 106, 423

Afflerbach A., Churchwell E., Werner M.W., 1997, ApJ 478, 190

Arnett D., 1996, In: Supernovae and Nucleosynthesis. Princeton University Press

Bahcall J.N., Pinsonneault M.H., 1995, Review of Modern Physics

Becker S.R., Butler K., 1988, A&A 201, 232

Becker S.R., Butler K., 1989, A&A 209, 244

Becker S.R., Butler K., 1990, A&A 235, 326

Becker W., Fenkart R.P., 1971, A&AS 4, 241

Bertelli G., Bressan A., Chiosi C., Fagotto F., Nasi E., 1994, A&A 106, 275

Brown P.J.F., Dufton P.L., Lennon D.J., Keenan F.P., 1986a, MNRAS 220, 1003

Brown P.J.F., Dufton P.L., Lennon D.J., Keenan F.P., Kilkenny D., 1986b, A&A 155, 113

Butler K., 1984, Ph.D. Thesis, University of London

Cameron L.M., 1985, A&A 147, 47

Carraro G., Chiosi C., 1994, A&A 287, 761

Christian C.A., Smith H.A., 1983, PASP 95, 169

Crawford D.L., Barnes J.V., 1970, AJ 75, 952

Cunha K., Lambert D.L., 1994, ApJ 426, 170

Dennissenkov P.A., 1994, A&A 287, 113

de Vaucouleurs G., Pence W.D., 1978, AJ 83, 1163

Dopita M.A., Ryder S.D., 1994 ApJ 430, 163

Dufton P.L., 1979, A&A 73, 203

Dufton P.L., Brown P.F.J., Fitzsimmons A., Lennon D.J., 1990a, A&A 232, 431

Dufton P.L., Fitzsimmons A., Howarth.I.D., 1990b, ApJ 362, L59

Dufton P.L., Fitzsimmons A., Rolleston W.R.J., 1994, A&A 286, 449

Eber F., Butler K., 1988, A&A 202, 153

Edmunds M.G., Greenhow R.M., 1995, MNRAS 272, 241

Edvardsson B., Andersen J., Gustafsson B., et al., 1993, A&A 275, 101

Fich M., Silkey M., 1991, ApJ 366, 107

Fitzsimmons A., 1993, A&AS 99, 15

Fitzsimmons A., Brown P.J.F., Dufton P.L., Lennon D.J., 1990, A&A 232, 437

Fitzsimmons A., Dufton P.L., Rolleston W.R.J., 1992, MNRAS 259, 489

Fliegner J., Langer N., Venn K.A., 1996, A&A 308, L13

Friel E.D., Janes K.A., 1993, A&A 267, 75

Garnett D.R., Shields G.A., Skillman E.D., Sagan S.P., Dufour R.J., 1997, ApJ 489, 36

Garnett D.R., Shields G.A., Peimbert M., et al., 1999, ApJ 513, 168

Gehren T., Nissen P.E., Kudritzki R.P., Butler K., 1985, In: Danziger I.J., Matteucci F., Kjaer K. (eds.) Proc. ESO Workshop on Production and Distribution of CNO Elements. p. 171

Giddings J.R., 1981, Ph.D. Thesis, University of London

Gies D.R., Lambert D.L., 1992, ApJ 387, 673

Grevesse N., Noels A., 1993, In: Prantzos N., Vangioni-Flam E., Casse M. (eds.) Origin and Evolution of the Elements. Cambridge University Press, Cambridge, p. 14

Gummersbach C.A., Kaufer A., Schäfer D.R., Szeifert T., Wolf B., 1998, A&A 338, 881

Gustafsson B., Karlsson T., Olsson E., Edvardsson B., Ryde N., 1999, A&A 342, 426

Güsten R., Metzger P.G., 1982, Vistas Astr. 26, 159

Hambly N.C., Rolleston W.R.J., Keenan F.P., Dufton P.L., Saffer R.A., 1997, ApJS 111, 419

Hardorp J., Scholz M., 1970, ApJ 154, 1111

Harris H.C., 1981, AJ 86, 707

Henning T., Gürtler J., 1986, Ap&SS 128, 199

Henry R.B.C., Howard J.W., 1995, ApJ 438, 170

Hibbens R.E., Dufton P.L., Smartt S.J., Rolleston W.R.J., 1998 A&A 332, 681

Hubeny I., 1988, Computer Physics Comm. 52, 103

Janes K.A., 1979, ApJS 39, 135

Jeffery C.S., 1996, QJRAS 37, 39

Kaufer A., Szeibert Th., Krenzin R., Baschek B., Wolf B., 1994, A&A 289, 740

Kilian-Montenbruck J., Gehren T., Nissen P.E., 1994, A&A 291, 757

Knude H., 1992, A&AS 92, 841

Kraft R.P., Sneden C., Smith G.H., et al., 1997, AJ 113, 279

Kurucz R.L., 1979, ApJS 40, 1

Kurucz R.L., 1991, In: Philip A.G., Upgren A.R., Janes P.L. (eds.) Precision Photometry: Astrophysics of the Galaxy. L. Davis Press, Schenectady, p. 27

Lennon D.J., Dufton P.L., 1983, MNRAS 203, 443

Lennon D.J., Dufton P.L., Fitzsimmons A., Gehren T., Nissen P.E., 1991, A&A 240, 349

Lennon D.J., Dufton P.L., Mazzali P.A., Pasian F., Marconi G., 1996, A&A 314, 243

Luck R.E., 1982, ApJ 256, 177

Maciel W.J., Köppen J., 1994, A&A 282, 436

Maciel W.J., Quireza, 1999, A&A 345, 629

Maeder A., 1992, A&A 264, 150

Matteucci F., Francois P., 1989, MNRAS 239, 885

Mayor M., 1976, A&A 48, 301

Mayor M., Vigroux L., 1981, A&A 98, 1

McErlean N.D., Lennon D.J., Dufton P.L., 1999, A&A 349, 553

McWilliam A., 1997, ARA&A 35, 503

Meyer D.M., Jura M., Cardelli J.A., 1998, ApJ 493, 222

Mihalas D., Auer L.H., 1970, ApJ 160, 1161

Moffat A.F.J., Vogt N., 1975, A&AS 20, 85

Monteverde M.I., Herrero A., Lennon D.J., 2000, A&A, submitted

Napiwotzki R., Schönberner D., Wenkse V., 1993, A&A 268, 653

Pagel B.E.J., 1997, Nucleosynthesis and Chemical Evolution of Galaxies. Cambridge University Press, Cambridge

Pagel B.E.J., Edmunds M.G., 1981, ARA&A 19, 77

Panagi N., Tosi M., 1981, A&A 96, 306

Pasquali A., Perinotto M., 1993, A&A 280, 581

Peimbert M., Torres-Peimbert S., Rayo J.F., 1978, ApJ 220, 516

Peters G.J., 1976, ApJS 30, 551

Phillipps S., Edmunds M.G., 1991, MNRAS 251, 84

Pilyugin L.S., Edmunds M.G., 1996, A&A 313, 783

Portinari L., Chiosi C., 1999, A&A 350, 827

Portinari L., Chiosi C., 2000, A&A, submitted

Prantzos N., Aubert O., 1995, A&A 302, 96

Renzini A., Voli M., 1981, A&A 94, 175

Rolleston W.R.J., Brown P.J.F., Dufton P.L., Fitzsimmons A., 1993a, A&A 270, 107

Rolleston W.R.J., Dufton P.L., Fitzsimmons A., Howarth I.D., Irwin M.J., 1993b, A&A 277, 10

Rolleston W.R.J., Dufton P.L., Fitzsimmons A., 1994, A&A 284, 72

Rolleston W.R.J., Brown P.J.F., Dufton P.L., Howarth I.D., 1996, A&A 315, 95

Rolleston W.R.J., Hambly N.C., Dufton P.L., et al. 1997, MNRAS 290, 422

Rolleston W.R.J., Dufton P.L., McErlean N.D., Venn K.A., 1999, A&A 348, 728

Rudolph A.L., Simpson J.P., Haas M.R., Erickson E.F., Fich M., 1997, ApJ 489, 94

Searle L., 1971, ApJ 127, 17

Shaver P.A., McGee R.X., Newton L.M., Danks A.C., Pottasch S.R., 1983, MNRAS 204, 53

Shobbrook R.R., 1980, MNRAS 192, 821

Shobbrook R.R., 1983a, MNRAS 205, 1215

Shobbrook R.R., 1983b, MNRAS 205, 1229

Shobbrook R.R., 1984, MNRAS 206, 273

Simpson J.P., Colgan S.W.J., Rubin R.H., Erickson E.F., Haas M.R., 1995, ApJ 444, 721

Skillman E.D., 1998, In: Aparicio A., Herrero A., Sanchez F. (eds.) Stellar Astrophysics for the Local Group. Cambridge University Press, p. 457

Smartt S.J., 2000, In: Matteucci F., Giovanelli F. (eds.) The Roma-Trieste Workshop on: The Chemical Evolution of the Milky Way: Stars versus Clusters. Kluwer

Smartt S.J., Rolleston W.R.J., 1997, ApJ 481, L47

Smartt S.J., Dufton P.L., Rolleston W.R.J., 1996a, A&A 305, 164

Smartt S.J., Dufton P.L., Rolleston W.R.J., 1996b, A&AS 116, 483

Smartt S.J., Dufton P.L., Rolleston W.R.J., 1996c, A&A 310, 123

Sofia U.J., Cardelli J.A., Guerin K.P., Meyer D.M., 1997, ApJ 482, L105

Strobel A., 1991, A&A 247, 35

Thé P.S., Winter D., Feinstein A., Westerlund B.E., 1990, A&AS 82, 319

Torres-Peimbert S., Peimbert M., 1977, Rev. Mex. Astron. Astrofis. 2, 181

Turbide L., Moffat A.F.J., 1993, AJ 105, 1831

Twarog B.A., Ashman K.M., Anthony-Twarog B.J., 1997, AJ 114, 2556

van den Hoek L.B., de Jong T., 1997, A&A 318, 231

Venn K.A., 1999, ApJ 518, 405

Vila-Costas M.B., Edmunds M.G., 1993, MNRAS 265, 199

Vílchez J.M., Esteban C., 1996, MNRAS 280, 720

Vílchez J.M., Pagel B.E.J., Diaz A.I., Terlevich E., Edmunds M.G., 1988, MNRAS 235, 633